Advanced Robotics, Vol. 17, No. 9, pp. 837–862 (2003)

Also available online - www.vsppub.com

Full paper

Kinematic optimal design of a new parallel-type rolling mill: paramill

KEUM-SHIK HONG [1,*], KYUNG-TAE HONG [1], CHINTAE CHOI [2] and WAN-SUK YOO [1]

[1] *School of Mechanical Engineering, Pusan National University, 30 Jangjeon-dong, Geumjeong-gu, Busan 609-735, South Korea*
[2] *Process Research Team, RIST, Gwangyang 545-090, South Korea*

Received 3 September 2002; revised 18 March 2003; accepted 28 May 2003

Abstract—In this paper, a kinematic optimal design of a new parallel-type rolling mill based upon two Stewart platform manipulators is investigated. To provide the end-effector (work roll) with sufficient d.o.f. and to achieve the structural stability of each stand, a parallel manipulator with six legs is considered. The objective of this new parallel-type rolling mill is to pursue an integrated control of the strip thickness, strip shape, pair-crossing angle, uniform wear of the rolls and strip tension. By splitting the weighted Jacobian matrices into two parts, the linear velocity, angular velocity, force and moment transmissibilities are analyzed. A manipulability measure, as the ratio of the manipulability ellipsoid volume and the condition number of a split Jacobian matrix, is defined. The two kinematic parameters, the radius of the base and the angle between two neighboring joints, are optimally designed by maximizing the global force manipulability measure defined in the entire workspace. The maximum exerting force needed in hydraulic actuators is also calculated using the kinematic structure determined and the Plücker coordinates introduced. Simulation results are provided.

Keywords: Rolling mill; parallel manipulator; Stewart platform; Jacobian matrix; manipulability; kinematic optimality.

1. INTRODUCTION

Around the end of the 17th century, the first use of a rolling mill, which was composed of two cylindrical rolls, to make steel strips was found in England [1]. Until the 18th century, the waterwheel was used as a power source for the mills. Gradually, steam engines replaced the waterwheels and considerably enhanced the production capability of the mills. The industrial revolution in the 19th century gave a further impetus toward the automated hot rolling process. At the beginning of the

*To whom correspondence should be addressed. E-mail: kshong@pusan.ac.kr

20th century, steam engines had been substituted by electric motors. Figure 1 shows a multi-stand continuous rolling process, which is widely used in the current steel making industry.

Figure 2 shows an operation schematic of the work and backup rolls of a stand. Each stand consists of two sets of work and backup rolls. The purpose of a backup roll is to support the work roll during the rolling process. Both rolls, as a unit, can move up and down for the purpose of adjusting the thickness of the strip. Because the middle section of the strip is less compressed than the side edges of the strip

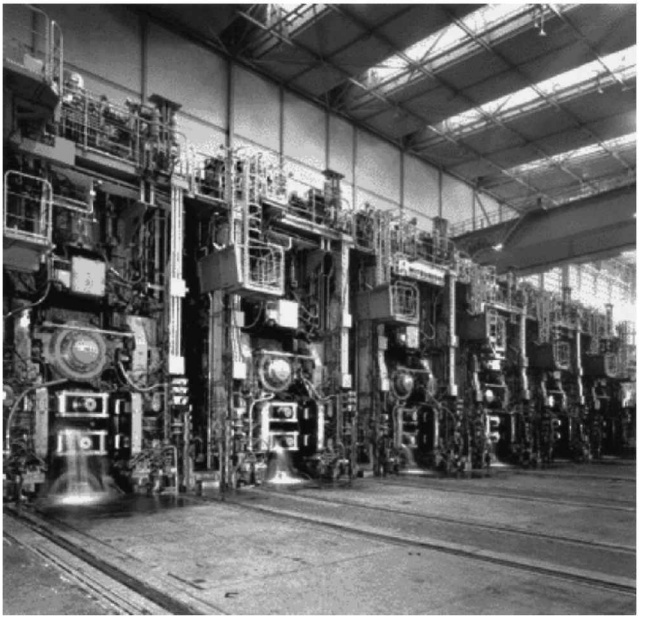

Figure 1. The current multi-stand rolling process.

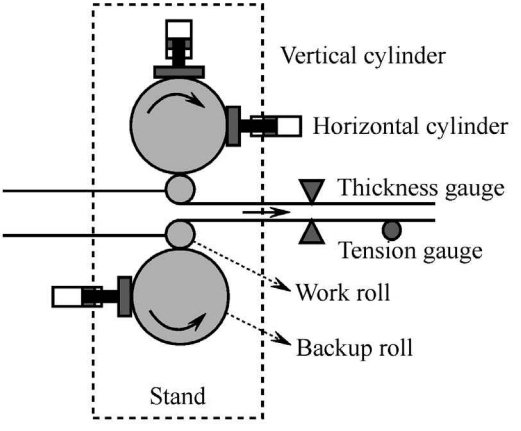

Figure 2. Operation schematic of a rolling mill.

due to the bending of the rolls, two sets of rolls are obliquely placed. This oblique placement of the rolls is called the pair-crossing, with which an even thickness across the strip is achieved. To adjust the pair-crossing angle of the rolls, two horizontal hydraulic cylinders are used. In the conventional mill, the each roll has 3 d.o.f.: heave, pair-crossing (yawing) and rolling.

With the current rolling technology, once the roll gap and the pair-crossing angle are set up, these cannot be modified during the process. Only the roll velocity and the looper angle for adjusting the strip tension can be changed. Therefore, concurrent control of the strip thickness, strip tension, strip shape and even wear of rolls is not possible. This necessitates the development of a new rolling technology, which can provide the work rolls with 6 d.o.f.

In this paper, a kinematic and dynamic optimal design of a new parallel-type rolling mill the 'paramill', is investigated. Note that a new rolling mill should provide at least 5-d.o.f. motions for the work roll: surge (strip tension control), sway (even wear across the roll), heave (strip thickness control), rolling (strip shape control) and yawing (even thickness across the strip) motions. The pitching motion of the roll is not critical because the roll itself is rotating. The paramill will make the looper mechanism unnecessary, which is currently used for controlling the strip tension, and will allow integrated control of the five motions.

The rolling process consumes a large amount of power and needs accurate control. The six hydraulic cylinders are located in parallel, so that the rolling force can be evenly distributed. Also, in comparison with a serial manipulator, the positioning accuracy of a parallel manipulator is better, the structural stiffness is high and the dynamic response time is also superior. On the other hand, the workspace of a parallel manipulator is relatively small. Such small workspace is an evident weakness in general; however, the paramill is well suited to the rolling process because the required workspace for rolling is quite small. The Stewart platform considered in this paper consists of, as usual, a platform, a base and six hydraulic cylinders. Hence, by attaching a work roll to the platform, 6-d.o.f. motions of the roll can be obtained. The advantages of having six legs rather than five legs are to improve the structural stability and to utilize existing knowledge in the area of a 6-d.o.f. motion simulator. Also, by evenly distributing the rolling force to six legs, a more compact stand than the case of five legs can be made. Of course, two Stewart platforms should face each other to press the strip in opposite directions.

The objective of this paper is to investigate a task-oriented structure of the Stewart platform for rolling. The design stage is divided into two stages. The first stage is a kinematic optimal design. In this part, the base radius and the joint arrangement of six hydraulic cylinders are determined for a given platform radius. The velocity-Jacobian matrix is derived from the kinematic relationship. A new manipulability measure, which is the ratio of the manipulability ellipsoid volume and the condition number of a split Jacobian matrix, is introduced. The two kinematic parameters, the base radius and the acute angle between two neighboring

joints are determined in the fashion that the manipulability measures in terms of force/moment transmissibilities are maximized.

The second stage is a dynamical optimal design. In this part, considering the maximum linear/angular acceleration of the roll and the maximum force/moment generated, the size of each hydraulic cylinder is determined for given mass and mass moment of inertia of the roll. Therefore, when the kinematic structure is pre-determined, the final specifications of the paramill are determined through the dynamic analysis.

The present paper makes the following contributions. This paper is the first paper investigating a different rolling technology with a new structure. A manipulability measure, as the ratio of the manipulability ellipsoid volume and the condition number of a velocity/force-Jacobian matrix, is defined. Two kinematic parameters, the base radius and the angle between neighboring joints, are optimally designed by maximizing the manipulability measure in the entire workspace. Also, the size of individual actuators is optimally designed by a dynamic analysis for the structure pre-selected and using the maximum force/moment generated in the rolling process. It is not the authors' intention to claim that the proposed structure is the best structure. The sole purpose is to stimulate the engineers in the steel-making industry and to look for a different way of making steel strips. Since some conceptual design results are also included in the paper, the engineers can determine whether it is feasible or not and hopefully come up with the best idea eventually.

This paper is organized as follows. Section 2 briefly describes the rolling process and presents the coordinate systems of the Stewart platform. A velocity-Jacobian matrix via kinematic analysis and a force-Jacobian matrix via the application of the principle of virtual work are derived. Also, the workspace needed for rolling is introduced. Section 3 discusses the determination of a kinematic structure. In Section 4, the analyzed results in Section 3 are applied to the dynamic analysis and then the required force needed at each hydraulic cylinder is determined. Finally, conclusions are given in Section 5.

2. PRELIMINARIES: ROLLING PROCESS AND PARAMILL STRUCTURE

In this section, to enhance understanding, the rolling process is briefly described. Also, the basic structure of the parallel mill, the derivation of Jacobian matrices and the workspace, in which all kinematic optimizations are performed, are presented.

2.1. Rolling process

Rolling is a mechanical process whereby plastic deformation of the metals is achieved by passing it between two rotating rolls. The main difference between hot and cold rolling is that in hot rolling the workpiece is initially at, or is heated to, above the recrystallization temperature, in contrasted to cold rolling, where the workpiece is initially at ambient temperature [2].

The process route can best be described in terms of the major items of equipment as follows [3, 4]. The feed stock for the rolling mill are slabs produced by the continuous casting process in a steel plant. Therefore, the slabs at ambient temperature are first sent to a reheat furnace to raise the temperature of the whole slab to around 1300°C. On exit from the reheat furnace, there is a buildup of scale on the surface of the slab, due to oxidation, which is detrimental to surface quality. This is removed within the de-scaling box, which consists of jets of high-pressure water. The slab is then sent to a roughing mill, which is a reversing mill that produces a breakdown bar by rolling the slab through a series of forward and reverse passes, typically reducing the slab thickness from 200 to 30 mm. After removing any variations in the leading edge of the breakdown bar and de-scaling, the slab is finally sent to a finishing mill, which is designed to reduce the thickness of the breakdown bar to that of the finished coil, while maintaining the desired width. A sequential combination of stands, from two to seven, is used depending on the product being rolled. The mill control system is critical, as constant mass flow must be maintained in all stands to ensure continuous production. On exiting the finishing mill, the product, which is typically above 800°C, is cooled at the run-out table. On exiting from the mill/run-out table cooling system, the hot product typically has a velocity of up to 40 m/h and can be hundreds of meters in length. The down coiler finally allows the product to be converted into a coil of dimensions that can be easily transported.

2.2. Paramill configuration and Jacobian

Figure 3 shows the kinematic configuration of a Stewart platform. It consists of a fixed base and a moving platform, which is connected to the base by variable six legs. By varying the lengths of the legs, the mechanism provides the platform with the 6 d.o.f. with respect to the base. Figure 4 shows the schematic of a stand using two sets of Stewart platforms. Figure 5 demonstrates a possible continuous rolling process, which uses seven new paramills. Figure 6 shows the joint arrangement for connecting the hydraulic cylinders on the base and on the platform. The arrangement in Fig. 6 can avoid the kinematic singularity [5–7]. This paper focuses on the design of one Stewart platform, because the same structure can be applied to all others.

For a given roll length, the design parameters are the radius of the base (r_b) and the angles between two adjacent joints, i.e. $2\phi_b$ and $2\phi_p$. Among the three variables $\{r_b, \phi_b, \phi_p\}$, $\phi_b = \phi_p$ is assumed, for brevity, by shrinking the design variables from three to two and allowing the three-dimensional (3D) plots in Figs 9 and 10. There is no imperative reason for choosing $\phi_b = \phi_p$. This is only the authors' choice. Therefore, a further investigation with different ϕ_b and ϕ_p may give different results. The r_b determined will decide the size of a stand.

In Fig. 3, let $X-Y-Z$ and $x-y-z$ denote a fixed coordinate system attached to the base and a moving coordinate system attached to the platform, respectively. Let the superscript 'p' denote the vectors represented in the platform coordinate. Therefore,

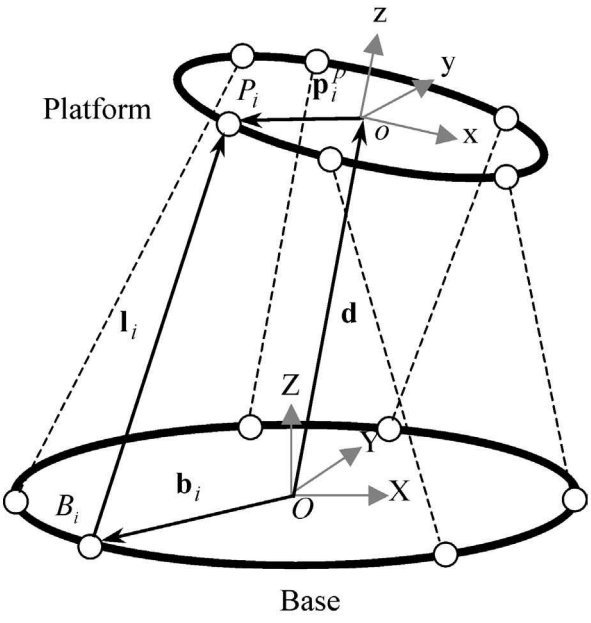

Figure 3. Schematic of the Stewart platform manipulator: coordinate systems.

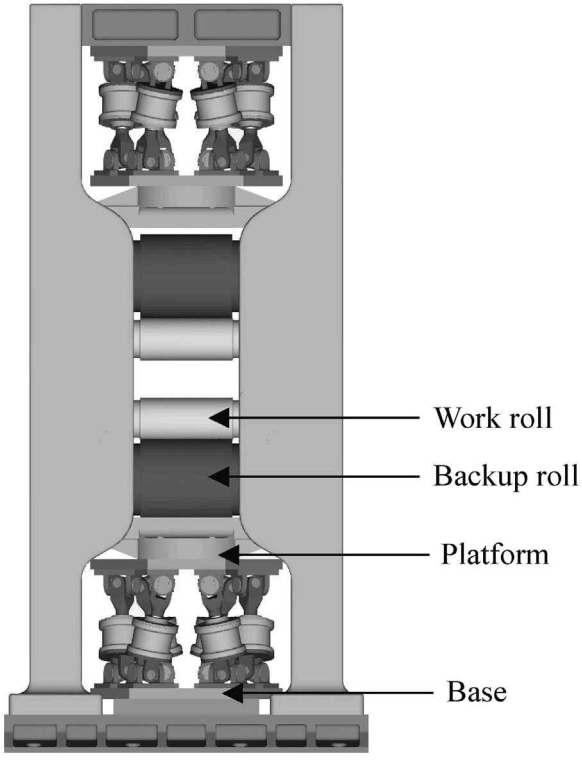

Figure 4. A new rolling mill using two Stewart platforms.

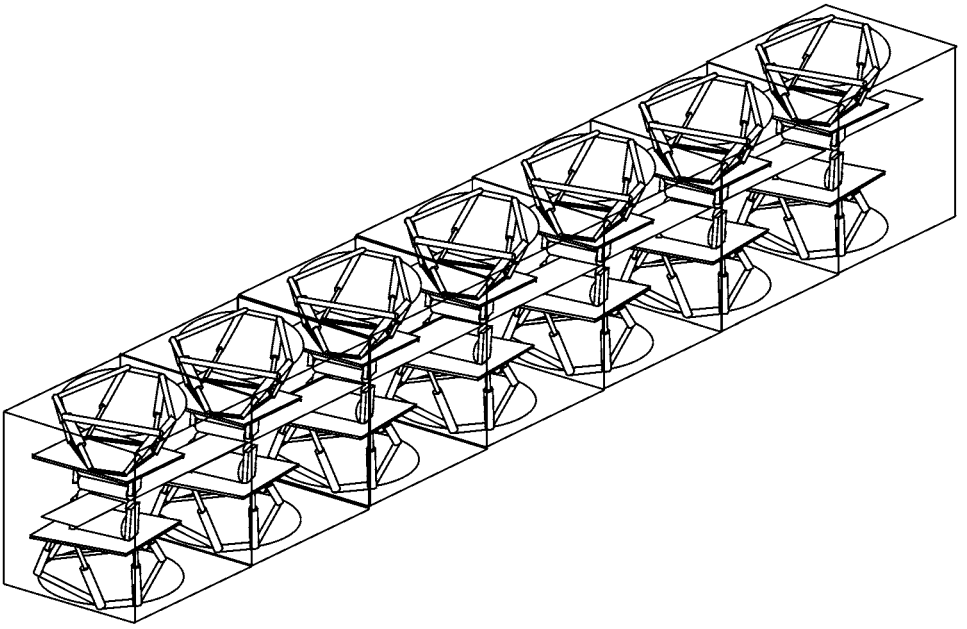

Figure 5. The proposed continuous rolling process using seven parallel rolling mills.

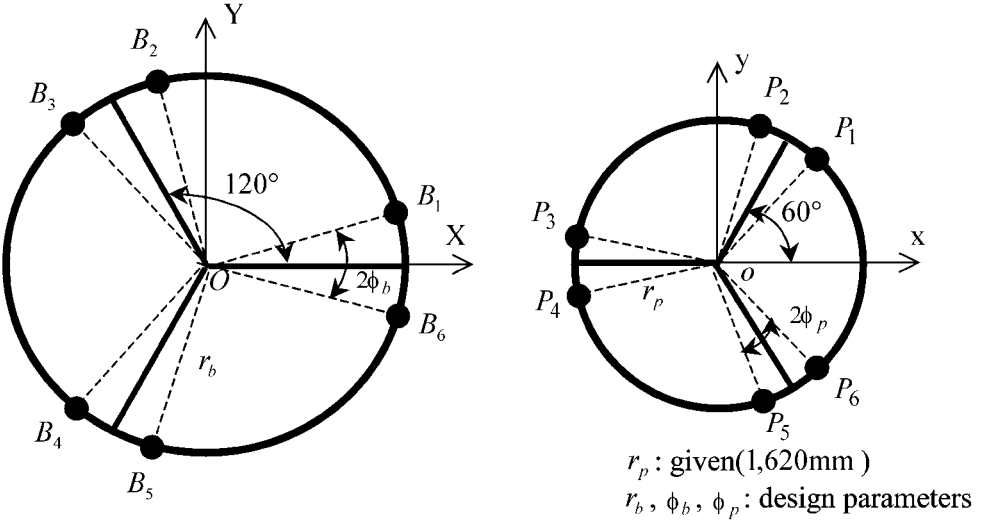

Figure 6. Joint locations on the base and platform.

the position vectors from two origins O and o to the joints are $\mathbf{b}_i = \overrightarrow{OB}_i$, $\mathbf{p}_i = \overrightarrow{OP}_i$ and $\mathbf{p}_i^{\mathrm{p}} = \overrightarrow{oP}_i$, $i = 1, 2, \ldots, 6$. The leg vectors are $\mathbf{l}_i = \overrightarrow{B_iP_i}$, $i = 1, 2, \ldots, 6$. Also, let $\mathbf{d} = \overrightarrow{Oo} = [d_X \; d_Y \; d_Z]^T$.

The rotation matrix R of the platform, in terms of $X-Y-Z$ fixed angles, is given by:

$$R = \mathrm{Rot}_Z(\theta_Z)\mathrm{Rot}_Y(\theta_Y)\mathrm{Rot}_X(\theta_X), \tag{1}$$

where θ_X, θ_Y and θ_Z denote the rotation angles about the X, Y and Z fixed coordinate axes, respectively, which are the rolling, pitching and yawing angles of the platform, respectively. By combining the rotation matrix R with $\mathbf{p}_i^{\mathrm{p}}$, the platform joint vectors are given by:

$$\mathbf{p}_i = \mathbf{d} + R\mathbf{p}_i^{\mathrm{p}}, \quad i = 1, 2, \ldots, 6. \tag{2}$$

Also, the leg vectors can be represented as follows:

$$\mathbf{l}_i = \mathbf{p}_i - \mathbf{b}_i = \mathbf{d} - \mathbf{b}_i + R\mathbf{p}_i^{\mathrm{p}}, \quad i = 1, 2, \ldots, 6. \tag{3}$$

The inner product of (3) yields:

$$\mathbf{l}_i \cdot \mathbf{l}_i = (\mathbf{d} - \mathbf{b}_i + R\mathbf{p}_i^{\mathrm{p}}) \cdot (\mathbf{d} - \mathbf{b}_i + R\mathbf{p}_i^{\mathrm{p}}), \quad i = 1, 2, \ldots, 6.$$

Let the length of the ith leg be $l_i = \|\mathbf{l}_i\|$. Then, the above equation becomes:

$$l_i^2 = (\mathbf{d} - \mathbf{b}_i + R\mathbf{p}_i^{\mathrm{p}}) \cdot (\mathbf{d} - \mathbf{b}_i + R\mathbf{p}_i^{\mathrm{p}}), \quad i = 1, 2, \ldots, 6. \tag{4}$$

Differentiating (4) with respect to time and using $\mathrm{d}/\mathrm{d}t(R\mathbf{p}_i^{\mathrm{p}}) = \boldsymbol{\omega} \times R\mathbf{p}_i^{\mathrm{p}}$ [8], the following expression is derived:

$$l_i\dot{l}_i = (\dot{\mathbf{d}} - \dot{\mathbf{b}}_i + \boldsymbol{\omega} \times R\mathbf{p}_i^{\mathrm{p}}) \cdot (\mathbf{d} - \mathbf{b}_i + R\mathbf{p}_i^{\mathrm{p}}), \quad i = 1, 2, \ldots, 6, \tag{5}$$

where $\boldsymbol{\omega} = [\omega_X\ \omega_Y\ \omega_Z]^T$ is the rotational angular velocity vector of the platform. Noting $\dot{\mathbf{b}}_i = \mathbf{0}$, the matrix representation of (5) becomes:

$$L\dot{\boldsymbol{\eta}} = K\dot{\boldsymbol{\xi}}, \tag{6}$$

where $\boldsymbol{\eta} = [l_1\ l_2\ l_3\ l_4\ l_5\ l_6]^T$, $\dot{\boldsymbol{\eta}} = [\dot{l}_1\ \dot{l}_2\ \dot{l}_3\ \dot{l}_4\ \dot{l}_5\ \dot{l}_6]^T$, $\boldsymbol{\xi} = [d_X\ d_Y\ d_Z\ \theta_X\ \theta_Y\ \theta_Z]^T$, $\dot{\boldsymbol{\xi}} = [\dot{d}_X\ \dot{d}_Y\ \dot{d}_Z\ \omega_X\ \omega_Y\ \omega_Z]^T$,

$$L = \begin{bmatrix} l_1 & 0 & 0 & 0 & 0 & 0 \\ 0 & l_2 & 0 & 0 & 0 & 0 \\ 0 & 0 & l_3 & 0 & 0 & 0 \\ 0 & 0 & 0 & l_4 & 0 & 0 \\ 0 & 0 & 0 & 0 & l_5 & 0 \\ 0 & 0 & 0 & 0 & 0 & l_6 \end{bmatrix}, \quad \text{and}$$

$$K = \begin{bmatrix} (\mathbf{d} - \mathbf{b}_1 + R\mathbf{p}_1^{\mathrm{p}})^T & [R\mathbf{p}_1^{\mathrm{p}} \times (\mathbf{d} - \mathbf{b}_1 + R\mathbf{p}_1^{\mathrm{p}})]^T \\ \vdots & \vdots \\ (\mathbf{d} - \mathbf{b}_6 + R\mathbf{p}_6^{\mathrm{p}})^T & [R\mathbf{p}_6^{\mathrm{p}} \times (\mathbf{d} - \mathbf{b}_6 + R\mathbf{p}_6^{\mathrm{p}})]^T \end{bmatrix}.$$

Also, let $\mathbf{v} = [\dot{d}_X \ \dot{d}_Y \ \dot{d}_Z]^T$ be the velocity vector of the origin of the moving coordinate. Then, the velocity relationship, between the actuators' length variation (leg velocity) and the translational linear velocity and rotational angular velocity of the platform, can be represented as follows:

$$\dot{\boldsymbol{\xi}} = \begin{bmatrix} \mathbf{v} \\ \boldsymbol{\omega} \end{bmatrix} = K^{-1} L \dot{\boldsymbol{\eta}} = J_{\mathrm{v}} \dot{\boldsymbol{\eta}}, \tag{7}$$

where $J_{\mathrm{v}} = K^{-1}L$ is defined as the velocity-Jacobian matrix. By adopting an incremental notation, (7) can be rewritten as:

$$\delta \boldsymbol{\xi} = J_{\mathrm{v}} \delta \boldsymbol{\eta}, \tag{8}$$

where $\delta \boldsymbol{\xi} = [\delta d_X \ \delta d_Y \ \delta d_Z \ \delta \theta_X \ \delta \theta_Y \ \delta \theta_Z]^T$ and $\delta \boldsymbol{\eta} = [\delta l_1 \ \delta l_2 \ \delta l_3 \ \delta l_4 \ \delta l_5 \ \delta l_6]^T$.

Now, by using the principle of virtual work, the relationship from the actuating forces of six hydraulic cylinders to the force and moment generated at the platform can be derived. Let the six actuating forces be $\mathbf{f} = [f_1 \ f_2 \ f_3 \ f_4 \ f_5 \ f_6]^T$, and the resultant force and moment at the platform be $\mathbf{F} = [F_x \ F_y \ F_z]^T$ and $\mathbf{M} = [M_x \ M_y \ M_z]^T$, respectively. Let $\boldsymbol{\tau} \stackrel{\Delta}{=} [\mathbf{F}^T \ \mathbf{M}^T]^T$. Then, the application of the principle of virtual work, i.e. the work done by constraint forces and external forces to the virtual displacement is zero, to the mechanism leads to [8]:

$$\mathbf{f}^T \delta \boldsymbol{\eta} - \boldsymbol{\tau}^T \delta \boldsymbol{\xi} = 0. \tag{9}$$

Substitution of (8) into (9) results in:

$$(\mathbf{f}^T - \boldsymbol{\tau}^T J_{\mathrm{v}}) \delta \boldsymbol{\eta} = 0. \tag{10}$$

Because the virtual displacements of the generalized coordinates ($\delta \boldsymbol{\eta}$) in (10) are independent, the following equation can be derived:

$$\mathbf{f} = J_{\mathrm{v}}^T \boldsymbol{\tau}. \tag{11}$$

Let $J_{\mathrm{f}} \stackrel{\Delta}{=} (J_{\mathrm{v}}^T)^{-1}$. Then, (11) can be rewritten as follows:

$$\boldsymbol{\tau} = J_{\mathrm{f}} \mathbf{f}, \tag{12}$$

where J_{f} is defined as the force-Jacobian matrix, which maps the actuating forces at six hydraulic cylinders to the force/moment generated at the platform. J_{v} in (7) and J_{f} in (12) will be used for input–output characterization in Section 3, because they represent the input–output characteristics, i.e. the translational linear velocity, the rotational angular velocity, the resultant force and moment of the end-effector with respect to given leg velocities and exerting forces at the legs. From $J_{\mathrm{f}} = (J_{\mathrm{v}}^T)^{-1}$, it can be seen that the two transmissibilities are not independent, i.e. although the input–output transmissibility of a velocity-Jacobian matrix is good, that of the associate force-Jacobian matrix may not be good depending on the configuration of the platform.

2.3. The workspace

In this subsection the workspace needed for rolling is briefly described. In a serial manipulator, the workspace, as a set of points in 3D space, is generally classified into a reachable workspace and a dexterous workspace. The reachable workspace is the set of all points that can be reached by the end-effector in at least one orientation, whereas the dexterous workspace is the set of all points reachable by the end-effector in all orientations. However, these definitions are not suitable in our case, because the dexterous workspace does not exist, i.e. it is not possible to rotate the platform completely upside down.

In this paper, two workspaces are defined: the position workspace and the orientation workspace. First, examining the translational distances and rotational angles of the work roll in the production line at KwangYang Works, South Korea, the position workspace, which represents the extent that the center point of the work roll can reach to, is defined as follows:

$$\Omega = \big\{(\Delta X, \Delta Y, \Delta Z) | -70 \leqslant \Delta X \leqslant 70,\ -100 \leqslant \Delta Y \leqslant 100, 0 \leqslant \Delta Z \leqslant 150; \text{ unit} = \text{mm}\big\}, \tag{13}$$

where ΔX, ΔY and ΔZ are incremental displacements of the work roll in the $X-Y-Z$ directions from the static equilibrium configuration. Also, at a given position of the roll, the orientation workspace, which represents how far the roll can rotates, is defined as follows:

$$\Delta = \big\{(\theta_X, \theta_Y, \theta_Z) | -1.42 \leqslant \theta_X \leqslant 1.42, \theta_Y = 0, -1 \leqslant \theta_Z \leqslant 1;\ \text{unit} = {}^\circ\big\}, \tag{14}$$

where θ_X, θ_Y and θ_Z are the rotational angles of the work roll in terms of fixed angles. Note that the pitching angle is zero in the orientation workspace. Table 1 summarizes 6 d.o.f. of the roll, their specifications and their control objectives.

Because the extent of the orientation workspace for rolling is very small, only the position workspace is mainly considered in the global manipulability analysis in Section 3. However, the orientation workspace is used in a later stage when determining the maximum/minimum lengths of six hydraulic cylinders.

3. KINEMATIC OPTIMAL DESIGN

3.1. Manipulability analysis

The focus of this section is to look for the 'optimal' kinematic configuration of the Stewart platform suitable for rolling process. The issue in this paper is not to find the best structure for rolling, but to determine how to configure the Stewart platform when it is used for rolling. Hence, upon the fulfillment of the desired workspace, one might want to know how easily the Stewart platform can be manipulated in terms of transmitting velocity and force [9–13]. That is, it would be desirable to

Table 1.
The workspace specifications used

6 d.o.f. motions		Upper and lower Stewart platform	Control objectives
Translational motions	Strip moving direction (surge)	±70 mm	strip tension control
	Roll sideward shift (sway)	±100 mm	uniform wear across the roll
	Strip thickness direction (heave)	150 mm	strip thickness control
Rotational motions	Rotation about the X-axis (rolling)	±1.42°	strip shape control
	Rotation about the Y-axis (pitching)	N/A	N/A
	Pair crossing (yawing)	±1°	uniform thickness across the roll

achieve the rolling objective in the Cartesian space with the use of minimal efforts in the joint space.

The two Jacobian matrices J_{v} in (7) and J_{f} in (12), which are functions of r (the base radius) and ϕ (the angle between two adjacent joints), map the joint velocities and joint forces in the joint space to the linear/angular velocity and the force/moment of the platform in the Cartesian space, respectively. Therefore, by configuring appropriate r and ϕ, the effect of velocity and force transmissions can be maximized. To analyze these input–output characteristics, the unit-norm inputs are often used, i.e. the unit sphere in the joint space is mapped to the Cartesian space [14]. However, these unit-norm inputs may not represent the actual operating range of the mechanism because the maximum velocity and maximum force of individual actuators may differ. Therefore, the normalization of individual actuator inputs by their maximum is preferred as follows:

$$\hat{\dot{\boldsymbol{\eta}}} \triangleq W_l^{-1}\dot{\boldsymbol{\eta}}, \tag{15}$$

$$\hat{\mathbf{f}} \triangleq W_f^{-1}\mathbf{f}, \tag{16}$$

where $W_l = \mathrm{diag}(\dot{l}_{1\,\max}, \dot{l}_{2\,\max}, \dot{l}_{3\,\max}, \dot{l}_{4\,\max}, \dot{l}_{5\,\max}, \dot{l}_{6\,\max})$ and $W_f = \mathrm{diag}(f_{1\,\max}, f_{2\,\max}, f_{3\,\max}, f_{4\,\max}, f_{5\,\max}, f_{6\,\max})$ represent the maximum velocities and maximum forces at six actuators, respectively, and $\hat{}$ denotes the normalized value.

In this paper, noting that the arrangement of the six hydraulic cylinders is symmetrical, it is assumed for brevity that the maximum velocities and forces of all actuators are equal. Thus, W_l and W_f can be taken as diagonal matrices with proper weightings. Substitution of (15) and (16) into (7) and (12), respectively, yields:

$$\begin{bmatrix} \mathbf{v} \\ \boldsymbol{\omega} \end{bmatrix} = (J_{\mathrm{v}} W_l)\hat{\dot{\boldsymbol{\eta}}}, \tag{17}$$

$$\begin{bmatrix} \mathbf{F} \\ \mathbf{M} \end{bmatrix} = (J_f W_f)\hat{\mathbf{f}}. \tag{18}$$

By splitting of (17) and (18) into two parts (see Ref. [15]), respectively, in terms of translational and rotational motions, we can obtain:

$$\begin{bmatrix} \mathbf{v} \\ \boldsymbol{\omega} \end{bmatrix} = \begin{bmatrix} \hat{J}_{\mathbf{v}\mathrm{o}} \\ \hat{J}_{\boldsymbol{\omega}\mathrm{o}} \end{bmatrix} \dot{\hat{\boldsymbol{\eta}}}, \tag{19}$$

$$\begin{bmatrix} \mathbf{F} \\ \mathbf{M} \end{bmatrix} = \begin{bmatrix} \hat{J}_{\mathbf{F}\mathrm{o}} \\ \hat{J}_{\mathbf{M}\mathrm{o}} \end{bmatrix} \hat{\mathbf{f}}, \tag{20}$$

where $\hat{J}_{\mathbf{v}\mathrm{o}}, \hat{J}_{\boldsymbol{\omega}\mathrm{o}}, \hat{J}_{\mathbf{F}\mathrm{o}}, \hat{J}_{\mathbf{M}\mathrm{o}} \in R^{3\times 6}$ and the subscript 'o' denotes 'output'. Since the analyses for all four split Jacobian matrices in (19) and (20) can be carried in the same fashion, a representative notation is used in the sequel.

Now, let $\hat{\mathbf{u}}$ and $\mathbf{q}$ denote a normalized input and an output, respectively. Then, (19) and (20) take the following single form:

$$\mathbf{q} = \hat{J}_{\mathrm{o}} \hat{\mathbf{u}}, \tag{21}$$

where $\hat{J}_{\mathrm{o}} \in \{\hat{J}_{\mathbf{v}\mathrm{o}}, \hat{J}_{\boldsymbol{\omega}\mathrm{o}}, \hat{J}_{\mathbf{F}\mathrm{o}}, \hat{J}_{\mathbf{M}\mathrm{o}}\}$, $\mathbf{q} \in \{\mathbf{v}, \boldsymbol{\omega}, \mathbf{F}, \mathbf{M}\}$, and $\hat{\mathbf{u}} \in \{\dot{\hat{\boldsymbol{\eta}}}, \hat{\mathbf{f}}\}$. Since the six columns of $\hat{J}_{\mathrm{o}}$ are not linearly independent (i.e. $\hat{J}_{\mathrm{o}}^{-1}$ does not exist), $\hat{\mathbf{u}}$ for a given $\mathbf{q}$ is not unique. Instead, the minimum norm solution with respect to a given $\mathbf{q}$ can be pursued. Let $\hat{J}_{\mathrm{o}}^{+}$ be the pseudoinverse of $\hat{J}_{\mathrm{o}}$ [16]. Then:

$$\hat{\mathbf{u}}^{+} = \hat{J}_{\mathrm{o}}^{+} \mathbf{q}, \tag{22}$$

where $\hat{\mathbf{u}}^{+}$ be the minimum norm solution. The pseudoinverse $\hat{J}_{\mathrm{o}}^{+}$ can be obtained from the singular value decomposition as follows:

$$\hat{J}_{\mathrm{o}}^{+} = H_{\mathrm{o}} \Sigma_{\mathrm{o}}^{+} G_{\mathrm{o}}^{T}, \tag{23}$$

where $G_{\mathrm{o}} = [\mathbf{g}_1\, \mathbf{g}_2\, \mathbf{g}_3]$ is the eigenvector matrix of $\hat{J}_{\mathrm{o}} \hat{J}_{\mathrm{o}}^{T} \in R^{3\times 3}$ and $H_{\mathrm{o}} = [\mathbf{h}_1\, \mathbf{h}_2\, \mathbf{h}_3\, \mathbf{h}_4\, \mathbf{h}_5\, \mathbf{h}_6]$ is that of $\hat{J}_{\mathrm{o}}^{T} \hat{J}_{\mathrm{o}} \in R^{6\times 6}$. G_{o} and H_{o} are orthogonal matrices. Also, $\Sigma_{\mathrm{o}}^{+} \in R^{6\times 3}$ is the transpose of $\Sigma_{\mathrm{o}} \in R^{3\times 6}$ which is composed of the reciprocal singular values of $\hat{J}_{\mathrm{o}}$. Because the actuator input vector $\hat{\mathbf{u}}$ has been normalized, the Euclidean norm of $\hat{\mathbf{u}}$ should satisfy the following inequality:

$$\|\hat{\mathbf{u}}\|^2 = \hat{\mathbf{u}}^{T} \hat{\mathbf{u}} \leqslant 1. \tag{24}$$

Also, $\hat{\mathbf{u}}^{+}$ should satisfy (24) because it is the minimum norm solution. Therefore, the substitution of (22) into (24) yields:

$$(\hat{\mathbf{u}}^{+})^{T} \hat{\mathbf{u}}^{+} = \mathbf{q}^{T} \left(\hat{J}_{\mathrm{o}}^{+^{T}} \hat{J}_{\mathrm{o}}^{+} \right) \mathbf{q} \leqslant 1. \tag{25}$$

By substituting (23) into (25), we can obtain the following relationship:

$$\mathbf{q}^{T} \left(\hat{J}_{\mathrm{o}}^{+^{T}} \hat{J}_{\mathrm{o}}^{+} \right) \mathbf{q} = \mathbf{q}^{T} \left(H_{\mathrm{o}} \Sigma_{\mathrm{o}}^{+} G_{\mathrm{o}}^{T} \right)^{T} \left(H_{\mathrm{o}} \Sigma_{\mathrm{o}}^{+} G_{\mathrm{o}}^{T} \right) \mathbf{q}$$

$$= \left(G_o^T \mathbf{q}\right)^T \left(\sum_o^{+^T} \sum_o^{+}\right) \left(G_o^T \mathbf{q}\right) \leqslant 1. \tag{26}$$

Let σ_1, σ_2 and σ_3 ($\sigma_1 > \sigma_2 > \sigma_3$) be the singular values of $\hat{J}_o$, and let $\bar{\mathbf{q}} \triangleq G_o^T \mathbf{q}$ where $\bar{\mathbf{q}} = [\bar{q}_1\ \bar{q}_2\ \bar{q}_3]^T$. Thus, the following ellipsoid equation is derived:

$$\frac{\bar{q}_1^2}{\sigma_1^2} + \frac{\bar{q}_2^2}{\sigma_2^2} + \frac{\bar{q}_3^2}{\sigma_3^2} \leqslant 1. \tag{27}$$

Now, (27) is named as the output manipulability ellipsoid for the weighted Jacobian matrix $\hat{J}_o$.

The above development is summarized as follows. For all possible normalized inputs satisfying $\|\hat{\mathbf{u}}\| \leqslant 1$, the maximum output is achieved in the direction of the first singular vector $\mathbf{g}_1$ of G_o which corresponds to the maximum singular value σ_1. Therefore, the maximum magnitude of output is σ_1 and in order to achieve this maximum output, the input $\hat{\mathbf{u}}$ should be applied in the direction of $\mathbf{h}_1 = \hat{J}_o^+(\sigma_1 \mathbf{g}_1)$. Similarly, the minimum output is achieved in the direction of the third singular vector $\mathbf{g}_3$ of G_o which corresponds to the minimum singular value σ_3. The magnitude of this output is σ_3 and the applied input $\hat{\mathbf{u}}$ in this case is $\mathbf{h}_3 = \hat{J}_o^+(\sigma_3 \mathbf{g}_3)$. Therefore, the output range for all inputs satisfying $\|\hat{\mathbf{u}}\| \leqslant 1$ becomes:

$$\sigma_3 \leqslant \|\mathbf{q}\| \leqslant \sigma_1. \tag{28}$$

Finally, let $\mathbf{q}_d$ be the desired output and μ be the maximum input–output transmissibility in that direction defined by $\bar{\mathbf{q}} \triangleq \mu G_o^T \mathbf{q}_d$. Then, the maximum transmissibility μ is obtained by substituting the above relationship into (27) as follows:

$$\mu = \left(\frac{\bar{q}_{d1}^2}{\sigma_1^2} + \frac{\bar{q}_{d2}^2}{\sigma_2^2} + \frac{\bar{q}_{d3}^2}{\sigma_3^2}\right)^{-1/2}, \tag{29}$$

where $\bar{\mathbf{q}}_d \triangleq G_o^T \mathbf{q}_d$.

Intuitively, the manipulability can be defined as how easily and uniformly the end-effectors are able to move in arbitrary directions. To analyze the manipulability of the mechanism, the manipulability ellipsoid is the most intuitive and useful measure. It can be made by mapping a unit sphere in the input space to the output space through the Jacobian matrix. The major and minor axes of the ellipsoid indicate the directions in which the platform can move most and least easily, and the ease is proportional to the principal axis length. Also, the magnitude and direction of the major and minor axes can be obtained from the singular value decomposition as described above. If the ellipsoid is larger and more circular, then the platform has faster velocity, larger forces and more uniform motion.

First, the volume of an output manipulability ellipsoid (MEV) and the condition number (CN) for a given weighted Jacobian matrix are defined as follows [17]:

$$\mathrm{MEV} \triangleq \frac{\pi^{\frac{\nu}{2}}}{\Gamma(1+\frac{\nu}{2})} \prod_{i=1}^{\nu} \sigma_i, \tag{30}$$

$$\mathrm{CN} \triangleq \frac{\sigma_{\max}}{\sigma_{\min}}, \tag{31}$$

where ν is the dimension of the manipulability ellipsoid and $\Gamma(\cdot)$ is the gamma function. The condition number represents the directional characteristics of the weighted Jacobian matrix. The larger the condition number is, the severer the directional characteristic. The larger the volume of the manipulability ellipsoid is, the greater the total output for a given input. Therefore, it is desirable to have a small condition number and a large volume. Therefore, both MEV and CN must be combined for a kinematic optimal design.

Now, the new manipulability measure is defined as follows:

$$\lambda(J_{\mathrm{o}}) \triangleq \frac{\text{Manipulability Ellipsoid Volume of } J_{\mathrm{o}}}{\text{Conditon Number of } J_{\mathrm{o}}} = \frac{\mathrm{MEV}(J_{\mathrm{o}})}{\mathrm{CN}(J_{\mathrm{o}})}. \tag{32}$$

Then, for the split weighted Jacobian matrices, individual manipulability measures can be defined as follows:

$$\lambda_1 \triangleq \frac{\mathrm{MEV}(\hat{J}_{\mathbf{v}\mathrm{o}})}{\mathrm{CN}(\hat{J}_{\mathbf{v}\mathrm{o}})}\text{: Translational Velocity Manipulability (TVM)},$$

$$\lambda_2 \triangleq \frac{\mathrm{MEV}(\hat{J}_{\boldsymbol{\omega}\mathrm{o}})}{\mathrm{CN}(\hat{J}_{\boldsymbol{\omega}\mathrm{o}})}\text{: Rotational Velocity Manipulability (RVM)},$$

$$\lambda_3 \triangleq \frac{\mathrm{MEV}(\hat{J}_{\mathbf{F}\mathrm{o}})}{\mathrm{CN}(\hat{J}_{\mathbf{F}\mathrm{o}})}\text{: Force Manipulability (FM)},$$

$$\lambda_4 \triangleq \frac{\mathrm{MEV}(\hat{J}_{\mathbf{M}\mathrm{o}})}{\mathrm{CN}(\hat{J}_{\mathbf{M}\mathrm{o}})}\text{: Moment Manipulability (MM)},$$

where subscripts $\mathbf{v}$, $\boldsymbol{\omega}$, $\mathbf{F}$ and $\mathbf{M}$ represent the translational velocity, the rotational angular velocity, force and moment, respectively. Note that all above manipulabilities are local, i.e. the value will be different at each point in the workspace. Therefore, integrating it over the entire workspace, the global manipulability can be defined as follows:

$$\Lambda_i = \frac{\int_{\Omega} \lambda_i(r_{\mathrm{b}}, \phi_{\mathrm{b}}, \phi_{\mathrm{p}})\, \mathrm{d}\Omega}{\int_{\Omega} \mathrm{d}\Omega}, \quad i = 1, 2, 3, 4, \tag{33}$$

where Ω, λ_i and Λ_i represent the entire workspace, the local manipulability measure and the global manipulability, respectively. Recall that $r_{\mathrm{b}}, 2\phi_{\mathrm{b}}$ and $2\phi_{\mathrm{p}}$ represent the base radius, angle between two joints on the base and that on

the platform, respectively. The platform radius was excluded because it can be determined by the size of a work roll.

Finally, it is noted that if the translational velocity manipulability is large, then the translational motion of the mechanism is fast and furthermore the response characteristics is uniform throughout the workspace. Similarly, if the force/moment manipulability is large, the mechanism can resist large external disturbance and the resistance characteristics are isotropic.

3.2. Determination of kinematic parameters

As an initial configuration of the work roll, let the distance between O and o be $\mathbf{d} = [0\ 0\ 0.8]^T$. Let the rotation matrix R be the identity matrix. Then, the position and orientation of the work roll can be expressed using the quantity deviated from the initial configuration.

Figures 7–10 show the 3D plots of the four global manipulabilities as functions of the base radius r_b and the joints angle $2\phi_b$. Figures 11 and 12 are the 2D contours of Figs 7 and 8, respectively. The ranges of r_b and $2\phi_b$ that maximize the four global manipulabilities are summarized in Table 2. As remarked in Table 2, it can be said that the global translational and rotational velocity manipulabilities are less important than the global force and moment manipulabilities for the case of a rolling mill. This is because an abrupt change of the strip thickness or the pair-crossing angle, i.e. a tracking problem, is not necessary. Instead, immediate control of the rolling force and moment may be needed. Therefore, in this paper, among the four manipulabilities introduced, the global force and moment manipulabilities are focused on in selecting the link parameters.

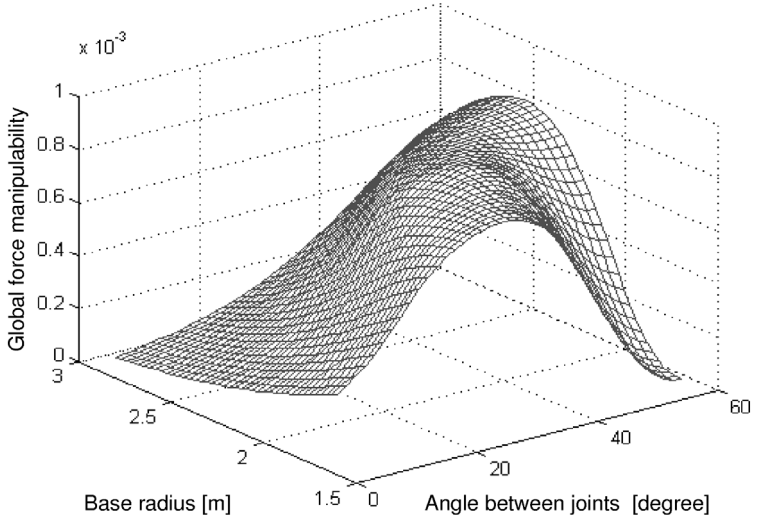

Figure 7. 3D plot of the global force manipulability measure.

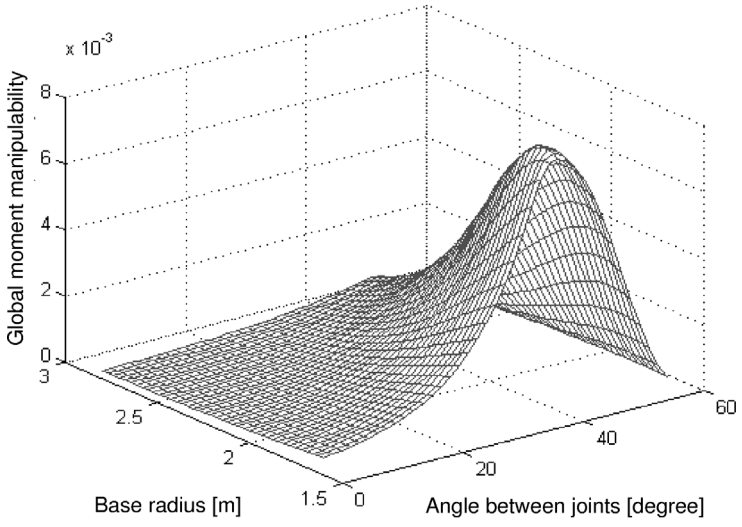

Figure 8. 3D plot of the global moment manipulability measure.

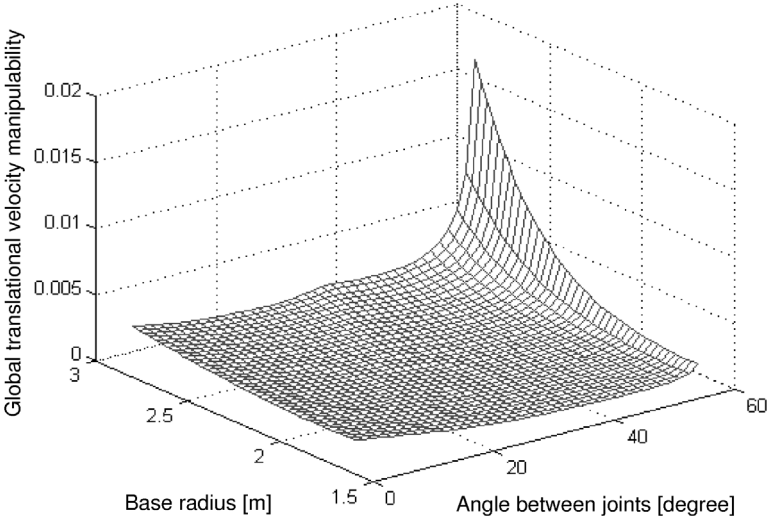

Figure 9. 3D plot of the global translational velocity manipulability measure.

For the computation of Figs 7–10, the following ranges of two kinematic parameters have been searched.

$$0 < 2\phi_b < 60^\circ,$$
$$1620 \leqslant r_b \leqslant 2850 \text{ mm}.$$

The 0° angle between two neighboring joints means that the two hydraulic cylinders are overlapped at one point and the 60° angle between two neighboring joints results in a singular configuration [5, 6]. Therefore, the angles of $0 < 2\phi_b < 60^\circ$ have been

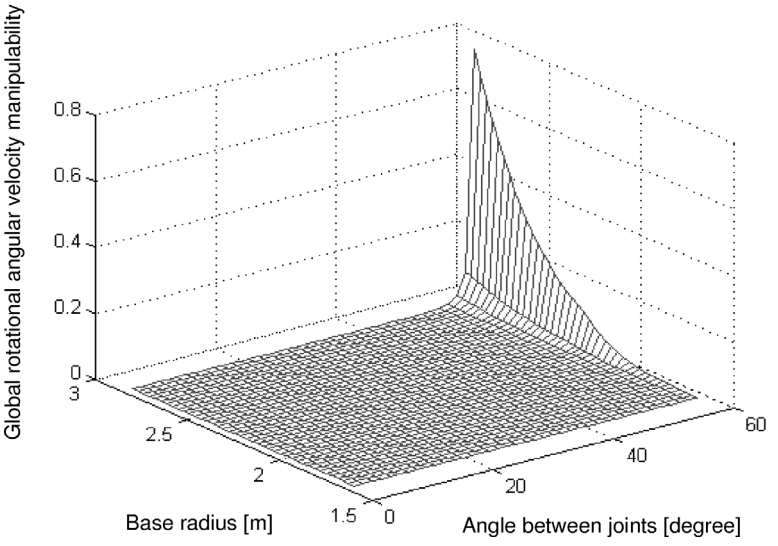

Figure 10. 3D plot of the global rotational angular velocity manipulability measure.

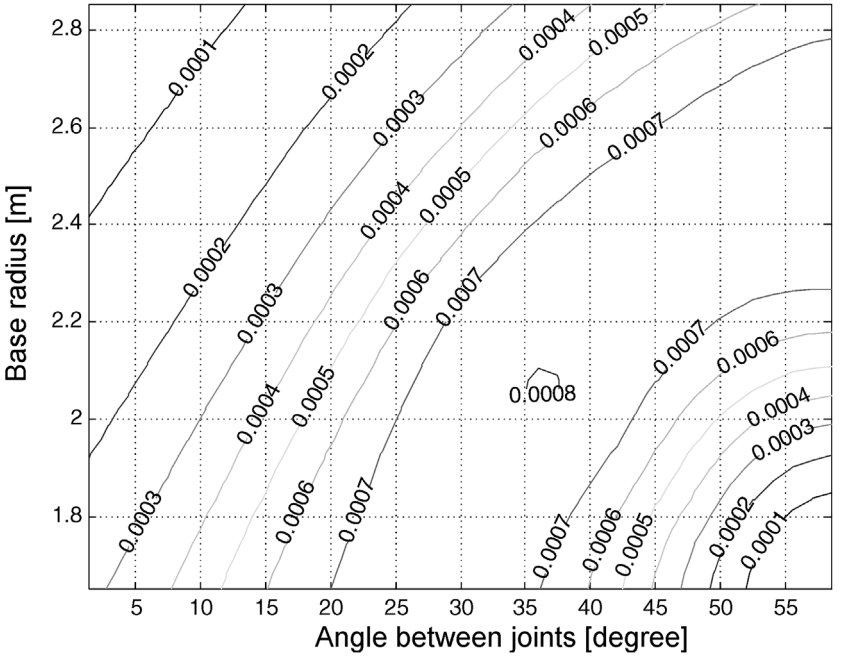

Figure 11. 2D contours of the global force manipulability measure.

considered. The fact that the length of a roll is 1620 mm implies that $r_b \geqslant 1620$ mm. Also, $r_b \leqslant 2850$ mm comes from the fact that the width of a stand is limited by 2850 mm. Because all the above values were taken for demonstration purpose, they

can be modified at a later stage to reflect the actual conditions. If the base radius and platform radius become identical, the moment manipulability is maximized.

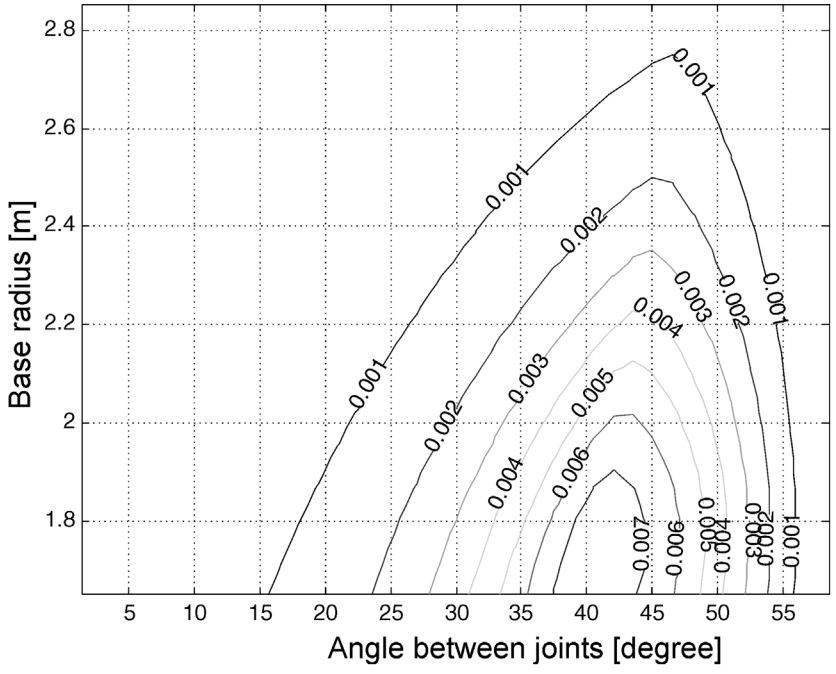

Figure 12. 2D contours of the global moment manipulability measure.

Table 2.
Link parameters optimized by the force manipulability measure

	r_b (mm)	$2\phi_b$ (°)	Remark
Global force manipulability	1800–2200	30–45	important
Global moment manipulability	1620–1950	37.5–44	important
Global translational velocity manipulability	2850	60	relatively less important
Global rotational angular velocity manipulability	2850	60	relatively less important

Table 3.
Final specifications based upon kinematic optimization

Platform radius (r_p)	Base radius (r_b)	Angle between joints ($2\phi_b = 2\phi_p$)	Minimum length of leg (l_{min})	Maximum length of leg (l_{max})
1620 mm	1900 mm	41°	907.7 mm	1269.3 mm

In summary, $\mathbf{d}$ and r_p are given; r_b and $2\phi_b$ have been determined by kinematic optimal design. Therefore, $\mathbf{b}_i$ and $\mathbf{p}_i^p$ can be determined from $\mathbf{d}, r_p, r_b$ and $2\phi_b$. Note also that a point in the orientation workspace can be characterized the rotation matrix R. Therefore, by varying R in (3), the maximum or minimum length of individual legs can be calculated. The final values determined by kinematic analysis are gathered in Table 3. Finally, it is remarked that the recommended values of the base radius and the angle between two neighboring joints are 1800–1950 mm and 37.5–44°, respectively.

4. DYNAMIC OPTIMAL DESIGN

4.1. Dynamic analysis

The objective of this section is to determine the maximum force needed in the actuator, and therefore the size of a hydraulic cylinder and the dimension of a universal joint can be determined. For a dynamic optimal design using the structure determined in Section 3, the Plücker coordinates [18] are introduced. With the use of the Plücker coordinates, the input force at a hydraulic cylinder and its moment can be easily represented in the platform coordinate. In Fig. 13, let $\mathbf{l}_i$ be $\overline{B_i P_i}$ and $\mathbf{l}_i^p$ be the vector $\mathbf{l}_i$ in the platform coordinates. Also, let $\mathbf{m}_i$ be the moment vector perpendicular to the plane made by $\mathbf{l}_i$ and the origin O. The moment vector $\mathbf{m}_i$ is defined as follows:

$$\mathbf{m}_i \triangleq \mathbf{b}_i \times \mathbf{p}_i, \quad i = 1, 2, \ldots, 6. \tag{34}$$

Also, the following relationships hold:

$$\mathbf{m}_i = \mathbf{b}_i \times \mathbf{l}_i = \mathbf{p}_i \times \mathbf{l}_i, \quad i = 1, 2, \ldots, 6. \tag{35}$$

The Plücker coordinates are defined, using (3) and (34), as follows:

$$\mathbf{s}_i = [l_{ix}\ l_{iy}\ l_{iz}\ m_{ix}\ m_{iy}\ m_{iz}],$$

where l_{ix}, l_{iy} and l_{iz} are three components of the vector $\mathbf{l}_i$ and m_{ix}, m_{iy} and m_{iz} are three components of the moment vector $\mathbf{m}_i$. Let the normalized vector of $\mathbf{l}_i$ be $\hat{\mathbf{l}}_i = \mathbf{l}_i / \|\mathbf{l}_i\|$ and the normalized moment of $\mathbf{m}_i$ be $\hat{\mathbf{m}}_i = \mathbf{m}_i / \|\mathbf{l}_i\|$, respectively. Then, the normalized Plücker coordinates become as follows:

$$\hat{\mathbf{s}}_i = [\hat{l}_{ix}\ \hat{l}_{iy}\ \hat{l}_{iz}\ \hat{m}_{ix}\ \hat{m}_{iy}\ \hat{m}_{iz}].$$

The reason for the normalization of the Plücker coordinates is because $\hat{\mathbf{l}}_i$ becomes the unit vector along the line $\overline{B_i P_i}$, therefore its scalar multiplication represents the force vector along the line and thus the vector $\hat{\mathbf{m}}_i$ is the moment about the origin of a unit force acting along the line [19].

In Fig. 13, since $\mathbf{l}_i^p = \mathbf{p}_i^p - \mathbf{b}_i^p$ and $\mathbf{b}_i = \mathbf{d} + R\mathbf{b}_i^p$, the following holds:

$$\mathbf{l}_i^p = \mathbf{p}_i^p + R^T(\mathbf{d} - \mathbf{b}_i), \quad i = 1, 2, \ldots, 6. \tag{36}$$

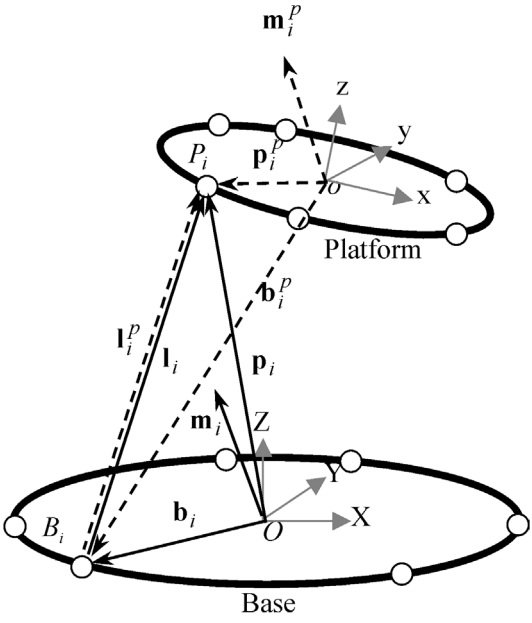

Figure 13. Plücker coordinates: solid line for the base and dotted line for the Platform.

By using the normal matrix property of R, i.e. $R^T R = I$:

$$\mathbf{l}_i^{\mathrm{p}} = R^T R\mathbf{p}_i^{\mathrm{p}} + R^T(\mathbf{d} - \mathbf{b}_i) = R^T(R\mathbf{p}_i^{\mathrm{p}} + \mathbf{d} - \mathbf{b}_i) = R^T\mathbf{l}_i. \tag{37}$$

Noting that $\mathbf{l}_i^{\mathrm{p}} \times \hat{\mathbf{l}}_i^{\mathrm{p}} = \mathbf{0}$ and $\mathbf{l}_i^{\mathrm{p}} = R^T\mathbf{l}_i$, $\hat{\mathbf{m}}_i^{\mathrm{p}}$ can be derived as follows:

$$\begin{aligned}\hat{\mathbf{m}}_i^{\mathrm{p}} &= \mathbf{p}_i^{\mathrm{p}} \times \hat{\mathbf{l}}_i^{\mathrm{p}} = \left[\mathbf{l}_i^{\mathrm{p}} + R^T(\mathbf{b}_i - \mathbf{d})\right] \times \hat{\mathbf{l}}_i^{\mathrm{p}} \\ &= \mathbf{l}_i^{\mathrm{p}} \times \hat{\mathbf{l}}_i^{\mathrm{p}} + R^T(\mathbf{b}_i - \mathbf{d}) \times \hat{\mathbf{l}}_i^{\mathrm{p}} = R^T(\mathbf{b}_i - \mathbf{d}) \times R^T\hat{\mathbf{l}}_i \\ &= R^T\left[(\mathbf{b}_i - \mathbf{d}) \times \hat{\mathbf{l}}_i\right] = R^T\left[(\mathbf{b}_i \times \hat{\mathbf{l}}_i) - (\mathbf{d} \times \hat{\mathbf{l}}_i)\right].\end{aligned} \tag{38}$$

Also, with $\mathbf{b}_i \times \hat{\mathbf{l}}_i = \hat{\mathbf{m}}_i$, (38) can be written as:

$$\hat{\mathbf{m}}_i^{\mathrm{p}} = R^T\left[\hat{\mathbf{m}}_i - (\mathbf{d} \times \hat{\mathbf{l}}_i)\right]. \tag{39}$$

Finally, the normalized Plücker coordinates vector can be represented with respect to the platform coordinates as follows:

$$\hat{\mathbf{s}}_i^{\mathrm{p}} = \left[\hat{l}_{ix}^{\mathrm{p}}\ \hat{l}_{iy}^{\mathrm{p}}\ \hat{l}_{iz}^{\mathrm{p}}\ \hat{m}_{ix}^{\mathrm{p}}\ \hat{m}_{iy}^{\mathrm{p}}\ \hat{m}_{iz}^{\mathrm{p}}\right].$$

Now, we assume that the mass and the mass moment of inertia of the actuators are relatively small compared with those of the platform including the rolls. Then, they can be ignored. Also, we assume that the input forces are generated by the pressure difference along the rod of the hydraulic cylinder. Figure 14 depicts a simplified structure of the platform. Let l_{w} and l_{b} be the length of the work and backup rolls, respectively. Let t be the thickness of the platform, and r_1 and r_2 be the radius of

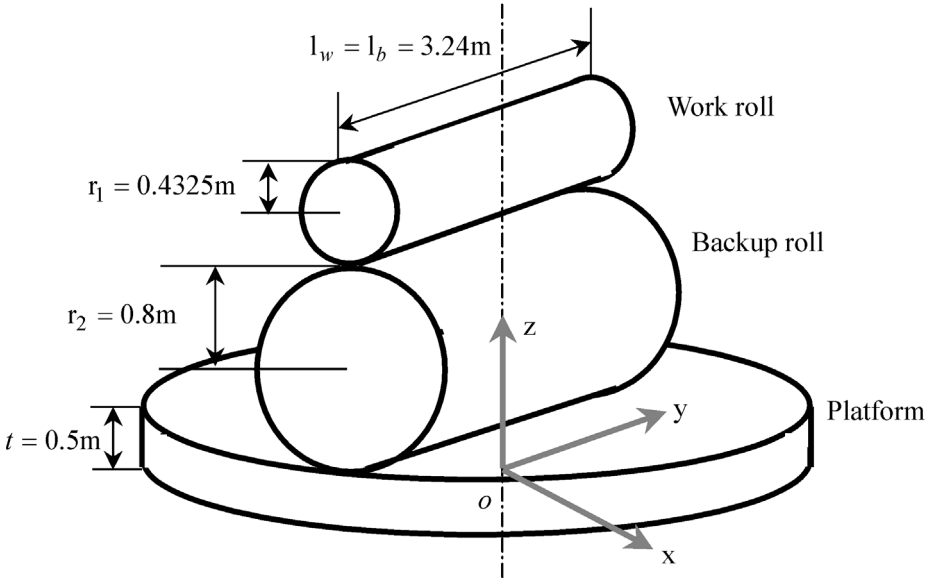

Figure 14. The platform structure used for dynamic optimization.

the work and backup rolls, respectively. Then, the force and moment equilibrium equations are:

$$\mathbf{F}_{\mathrm{G}}^{\mathrm{p}} + \mathbf{F}_{\mathrm{E}}^{\mathrm{p}} + \sum_{i=1}^{6} \mathbf{F}_i^{\mathrm{p}} = m\mathbf{a}, \tag{40}$$

$$\boldsymbol{\tau}_{\mathrm{E}}^{\mathrm{p}} + \sum_{i=1}^{6} \boldsymbol{\tau}_i^{\mathrm{p}} = \mathbf{I}^{\mathrm{p}}\boldsymbol{\alpha} + \boldsymbol{\omega} \times (\mathbf{I}^{\mathrm{p}}\boldsymbol{\omega}), \tag{41}$$

where m is the total mass of the platform structure ($m = m^{\mathrm{p}} + m_{\mathrm{b}} + m_{\mathrm{w}}$, where m^{p} is the platform mass, m_{b} is the backup roll mass and m_{w} is the work roll mass), $\mathbf{a}$ denotes the translational acceleration of the platform, $\mathbf{F}_{\mathrm{G}}^{\mathrm{p}}$ represents the weight of the platform, $\mathbf{F}_{\mathrm{E}}^{\mathrm{p}}$ denotes the external force on the platform including the vertical rolling force, the impact force due to the entrance of the strip and the tensile force along the strip, and $\mathbf{F}_i^{\mathrm{p}}$ denotes the input force at the ith actuator with magnitude f_i in the direction $\hat{\mathbf{l}}_i$. Also, $\boldsymbol{\tau}_{\mathrm{E}}^{\mathrm{p}}$ represents the resultant external torque, $\boldsymbol{\tau}_i^{\mathrm{p}}$ are the torques due to the actuating forces, $\boldsymbol{\alpha}$ represents the angular acceleration of the platform, $\boldsymbol{\omega}$ denotes the rotational angular velocity of the platform. Finally, $\mathbf{I}^{\mathrm{p}}$ is the mass moment of inertia of the platform in the platform coordinates given by:

$$\mathbf{I}^{\mathrm{p}} = \begin{bmatrix} I_{xx} & -I_{xy} & -I_{xz} \\ -I_{xy} & I_{yy} & -I_{yz} \\ -I_{xz} & -I_{yz} & I_{zz} \end{bmatrix},$$

where $I_{xy} = I_{yx} = 0$, $I_{xz} = I_{zx} = 0$ and $I_{yz} = I_{zy} = 0$. This is due to the fact that the platform structure is symmetric about the $x-z$ plane and the $y-z$ plane with respect to the origin o of the moving frame located in the center of the platform bottom. Also,

$$
\begin{aligned}
I_{zz} &= \frac{1}{2}m^{\mathrm{p}}\left\|\mathbf{p}_i^{\mathrm{p}}\right\|^2 + \frac{1}{12}m_{\mathrm{b}}(3r_2^2 + l_{\mathrm{b}}^2) + \frac{1}{12}m_{\mathrm{w}}\left(3r_1^2 + l_{\mathrm{w}}^2\right),\\
I_{yy} &= \frac{1}{12}m^{\mathrm{p}}\left(3\left\|\mathbf{p}_i^{\mathrm{p}}\right\|^2 + t^2\right) + m^{\mathrm{p}}\left(\frac{t}{2}\right)^2 + \frac{1}{2}m_{\mathrm{b}}r_2^2 + m_{\mathrm{b}}(t + r_2)^2 + \frac{1}{2}m_{\mathrm{w}}r_1^2,\\
&\quad + m_{\mathrm{w}}(t + 2r_2 + r_1)^2\\
I_{xx} &= \frac{1}{12}m^{\mathrm{p}}\left(3\left\|\mathbf{p}_i^{\mathrm{p}}\right\|^2 + t^2\right) + m^{\mathrm{p}}\left(\frac{t}{2}\right)^2 + \frac{1}{12}m_{\mathrm{b}}\left(3r_2^2 + l_{\mathrm{b}}^2\right) + m_{\mathrm{b}}(t + r_2)^2\\
&\quad + \frac{1}{12}m_{\mathrm{w}}\left(3r_1^2 + l_{\mathrm{w}}^2\right) + m_{\mathrm{w}}(t + 2r_2 + r_1)^2.
\end{aligned}
$$

Here, assuming that the material of the platform, backup roll and work roll is steel, ρ_{s} is $7850\,\mathrm{kg/m^3}$. Then,

$$
\begin{aligned}
m &= m^{\mathrm{p}} + m_{\mathrm{b}} + m_{\mathrm{w}} = 9.8445 \times 10^4\ \mathrm{kg}\ \text{and}\\
\mathbf{I}^{\mathrm{p}} &= \begin{bmatrix} 1.0916 & 0 & 0\\ 0 & 2.2397 & 0\\ 0 & 0 & 2.7290 \end{bmatrix} \times 10^5\ \mathrm{kg\,m^2},
\end{aligned}
$$

can be assumed. Now, (40) and (41) can be represented as follows:

$$
\left[\hat{\mathbf{l}}_1^{\mathrm{p}}\ \hat{\mathbf{l}}_2^{\mathrm{p}}\ \hat{\mathbf{l}}_3^{\mathrm{p}}\ \hat{\mathbf{l}}_4^{\mathrm{p}}\ \hat{\mathbf{l}}_5^{\mathrm{p}}\ \hat{\mathbf{l}}_6^{\mathrm{p}}\right]\mathbf{f} = \sum_{i=1}^{6}\mathbf{F}_i^{\mathrm{p}} = m\mathbf{a} - \mathbf{F}_{\mathrm{G}}^{\mathrm{p}} - \mathbf{F}_{\mathrm{E}}^{\mathrm{p}}, \tag{42}
$$

$$
\left[\hat{\mathbf{m}}_1^{\mathrm{p}}\ \hat{\mathbf{m}}_2^{\mathrm{p}}\ \hat{\mathbf{m}}_3^{\mathrm{p}}\ \hat{\mathbf{m}}_4^{\mathrm{p}}\ \hat{\mathbf{m}}_5^{\mathrm{p}}\ \hat{\mathbf{m}}_6^{\mathrm{p}}\right]\mathbf{f} = \sum_{i=1}^{6}\boldsymbol{\tau}_i^{\mathrm{p}} = \mathbf{I}^{\mathrm{p}}\boldsymbol{\alpha} + \boldsymbol{\omega} \times (\mathbf{I}^{\mathrm{p}}\boldsymbol{\omega}) - \boldsymbol{\tau}_{\mathrm{E}}^{\mathrm{p}}. \tag{43}
$$

Finally, (42) and (43) can be combined into a single equation by using the Plücker coordinates as follows:

$$
U\mathbf{f} = E, \tag{44}
$$

where: $U = \begin{bmatrix} \hat{\mathbf{l}}_1^{\mathrm{p}} & \hat{\mathbf{l}}_2^{\mathrm{p}} & \hat{\mathbf{l}}_3^{\mathrm{p}} & \hat{\mathbf{l}}_4^{\mathrm{p}} & \hat{\mathbf{l}}_5^{\mathrm{p}} & \hat{\mathbf{l}}_6^{\mathrm{p}} \\ \hat{\mathbf{m}}_1^{\mathrm{p}} & \hat{\mathbf{m}}_2^{\mathrm{p}} & \hat{\mathbf{m}}_3^{\mathrm{p}} & \hat{\mathbf{m}}_4^{\mathrm{p}} & \hat{\mathbf{m}}_5^{\mathrm{p}} & \hat{\mathbf{m}}_6^{\mathrm{p}} \end{bmatrix} \in R^{6\times 6}$

and

$$
E = \begin{bmatrix} m\mathbf{a} - \mathbf{F}_{\mathrm{G}}^{\mathrm{p}} - \mathbf{F}_{\mathrm{E}}^{\mathrm{p}} \\ \mathbf{I}^{\mathrm{p}}\boldsymbol{\alpha} + \boldsymbol{\omega} \times (\mathbf{I}^{\mathrm{p}}\boldsymbol{\omega}) - \boldsymbol{\tau}_{\mathrm{E}}^{\mathrm{p}} \end{bmatrix} \in R^{6\times 1}.
$$

U is determined from the kinematic structure, $\mathbf{f}$ is the input forces on the hydraulic cylinders and E contains external forces, inertia forces, gravity forces, external torques and inertia torques.

Table 4.
Final specifications based upon dynamic optimization

Hydraulic cylinder rod (mm)	Hydraulic cylinder outer diameter (mm)	Hydraulic cylinder outer diameter diameter (mm)	Universal joint cross axis (mm)	Yoke width (mm)	Yoke thickness (mm)
364	789.6	653.4	343	686	152

4.2. Determination of dynamic parameters

Once the maximum force is estimated, the universal joint needed for the connection of the base and a cylinder can be designed. The forces and torques generated in a rolling process are assumed as follows:

The vertical rolling force is 4000 ton, the external force is 100 ton and the external torque due to the external force is 100×2.965 ton m. We also assume that the velocity and the acceleration of the platform are 1 m/s and 1 m/s^2, respectively, and that the angular velocity and the angular acceleration of the platform are 1 rad/s and 1 rad/s^2, respectively. It is noted that the roll torque is not included as an external torque of the platform.

Now, by using (44), the maximum force is estimated to be 1250 ton. This is the maximum force that a hydraulic cylinder has to resist. The final specifications of the parts of a hydraulic cylinder and a universal joint based upon the above analysis are listed in Table 4. The detailed mechanical design procedures in Table 4 are all skipped due to the length of the paper and are an easy task for mechanical engineers. The sole purpose of Table 4 is just to give an idea on how large a cylinder and an universal joint should be.

5. CONCLUSIONS

This paper has investigated a feasibility study on a new parallel-type rolling mill utilizing two Stewart platforms. The main objective of this new rolling mill is to provide an integrated control of the strip thickness, even wear across the roll, strip tension, uniform thickness across the strip and strip shape. For a given platform radius, the base radius and the angle between two adjacent joints of the base/platform were determined by maximizing the global force manipulability measure newly defined, which is the ratio of the manipulability ellipsoid volume and the condition number of the force-Jacobian matrix defined in the entire workspace. Then, the determined kinematic structure was used to decide the capacity of hydraulic actuators through the dynamic design. As future research, because $\phi_b = \phi_p$ among the three design variables $\{r_b, \phi_b, \phi_p\}$ has been assumed in this paper, a further investigation using different values of ϕ_b and ϕ_p would be interesting. The proposed method is generic in the sense that it can be applied to any situation where the output needs to be maximized for the given inputs.

Acknowledgements

This work was supported by the Ministry of Science and Technology of Korea under the grant of National Research Laboratory.

REFERENCES

1. W. L. Roberts, *Hot Rolling of Steel.* Marcel Dekker, New York, NY (1983).
2. E. M. Mielnik, *Metalworking Science and Engineering.* McGraw-Hill, New York, NY (1991).
3. Y. Bissessur, E. B. Martin, A. J. Morris and P. Kitson, Fault detection in hot steel rolling using neural networks and multivariate statistics, *IEE Proc. Control Theory Appl.* **147** (6) (2000).
4. K. S. Hong, J. G. Kim and M. Tomizuka, Control of strip casting process: decentralization and optimal roll force control, *Control Eng. Practice* **9** (9), 933–945 (2001).
5. C. M. Gosselin and J. Angeles, Singularity analysis of closed-loop kinematic chains, *IEEE Trans. Robotics Automat.* **6** (3), 281–290 (1990).
6. O. Ma and J. Angeles, Architecture singularities of platform manipulators, in: *IEEE Int. Conf. on Robotics and Automation*, Sacramento, CA, pp. 1542–1547 (1991).
7. F. C. Park and J. W. Kim, Singularity analysis of closed kinematic chains, *ASME Trans. J. Mech. Des.* **121** (1), 32–38 (1999).
8. M. W. Spong and M. Vidyasagar, *Robot Dynamics and Control.* Wiley, New York (1989).
9. T. Yoshikawa, Manipulability of robotic mechanisms, *Int. J. Robotics Res.* **4** (2), 3–9 (1985).
10. M. Uchiyama, Structures and characteristics of parallel manipulators, *Adv. Robotics* **8** (6), 545–557 (1994).
11. K. E. Zanganeh and J. Angeles, Kinematic isotropy and the optimum design of parallel manipulators, *Int. J. Robotics Res.* **16** (2), 185–197 (1997).
12. F. C. Park and J. W. Kim, Manipulability of closed kinematic chains, *ASME Trans. J. Mech. Des.* **120** (4), 542–548 (1998).
13. H. Yoshida, K. Inoue, T. Arai and Y. Mae, Mobile manipulation of humanoid robots, in: *Proc. IEEE/ASME Int. Conf. on Advanced Intelligent Mechatronics*, Como, Italy, pp. 266–271 (2001).
14. K. S. Hong and J. G. Kim, Manipulability analysis of a parallel machine tool: application to optimal link parameter design, *J. Robotics Syst.* **17** (8), 403–415 (2000).
15. K. Kosuge, M. Okuda, H. Kawamata and T. Fukuda, Input/output force analysis of parallel link manipulators, *Trans. JSME C* **60** (575), 134–140 (1994).
16. G. Strang, *Linear Algebra and Its Applications*, 3rd edn. Harcourt Brace Jovanovich, New York (1988).
17. B. J. Ahn and K. S. Hong, Force/moment transmissionability analysis of a parallel manipulator, *J. Korean Soc. Precision Eng.* **13** (4), 109–121 (1996).
18. K. H. Hunt, *Kinematic Geometry of Mechanisms.* Oxford University Press, Oxford (1978).
19. E. F. Fichter, A Stewart platform based manipulator: general theory and practical construction, *Int. J. Robotics Res.* **5** (2), 157–181 (1986).
20. J. J. Craig, *Introduction to Robotics*, 2nd edn. Addison Wesley, Reading, MA (1989).
21. J. P. Merlet, *Parallel Robots.* Kluwer, Dordrecht (2000).

ABOUT THE AUTHORS

Keum-Shik Hong received the BS degree in Mechanical Design and Production Engineering from Seoul National University in 1979, the MS degree in Mechanical Engineering from Columbia University, New York, in 1987, and both the MS degree in Applied Mathematics and the PhD degree in Mechanical Engineering from the University of Illinois at Urbana–Champaign (UIUC) in 1991. From 1991 to 1992, he was a Postdoctoral Fellow at UIUC. Dr. Hong is currently an Associate Professor in the School of Mechanical Engineering at Pusan National University, Korea. From 1979 to 1982, he served in the Korean Army, and from 1982 to 1985 he was with Daewoo Heavy Industries, Incheon, South Korea, where he worked on vibration, noise and emission problems of vehicles and engines. He served as an Associate Editor for the *Journal of Control, Automation and Systems Engineering* and the *Journal of the Korean Society of Precision Engineering.* He has been serving as an Associate Editor for *Automatica* since 2000 and as an Editor for the *International Journal of Control, Automation and Systems* since 2003. He is a member of ASME, IEEE, KSME, KSPE, KIEE and ICASE. His laboratory, Integrated Dynamics and Control Laboratory, was designated as a National Research Laboratory by the Ministry of Science and Technology of Korea in 2003. His research interests are in the areas of non-linear systems theory, adaptive control, distributed parameter system control, adaptive control and innovative control applications to engineering problems.

Kyung-Tae Hong received the BS degree in Electronic Communication Engineering from Kumoh National Institute of Technology, Gumi, South Korea, in 2000 and the MS degree in Mechatronics Engineering from Pusan National University, Busan, South Korea, in 2002. He is now a PhD student in the Department of Mechanical and Intelligent Systems Engineering at Pusan National University, Busan, South Korea. His research interests include adaptive control, crane system control, suspension system control, ECU development and embedded systems.

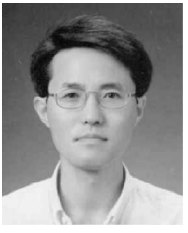

Chintae Choi received his BS, MS and PhD degrees in Mechanical Engineering at Pusan National University, South Korea, in 1982, 1984, and 1997, respectively. He is currently a Principal Researcher at the Research Institute of Industrial Science and Technology, Pohang, South Korea, since he joined it in 1986. He is also an Adjunct Professor in the Department of Electrical Engineering at Uiduk University, South Korea, where he teaches automatic control and mechatronics. During 1997–1998, he was a Postdoctoral Research Associate at the University of Illinois at Urbana–Champaign. His research interests include robust control, adaptive control and high accuracy positioning control for the hot rolling process in the steel industry.

Wan-Suk Yoo received the BS degree in Mechanical Engineering from Seoul National University in 1976, the MS degree in Mechanical Engineering from Korea Advanced Institute of Science and Technology in 1978 and the PhD degree in Mechanical Engineering from the University of Iowa in 1985. From 1978 to present, he has been with Pusan National University (PNU), South Korea. From 1994 to 1996, he served as an Associate Dean in the College of Engineering at PNU. From 1997 to the present, he has been serving as the Director of the Mechanical Engineering Technology and Research Information Center, South Korea. He is a member of ASME, SAE, KSME, KSPE, KSNVE and KSAE. His research interests are in the areas of flexible multibody dynamics, vehicle dynamics, and computer-aided modeling and

analysis of mechanical systems. His laboratory, CAElab at Pusan National University, was appointed as a National Research Laboratory by the Korean government in June 2002. He is now serving as a General Organizer of ACMD2004 (The Second Asian Conference on Multibody Dynamics), which will be held in August 2004 Seoul, South Korea.